Broadband asymmetric light transmission via all-dielectric digital metasurfaces

Bing Shen,[1] Randy Polson,[2] and Rajesh Menon[1,*]

[1]*Department of Electrical and Computer Engineering, University of Utah, Salt Lake City, Utah 84112, USA*
[2]*Utah Nanofabrication Facility, University of Utah, Salt Lake City, Utah 84112, USA*
[*]*rmenon@eng.utah.edu*

Abstract: We demonstrate broadband asymmetric transmission or optical-diode behavior via a digital metasurface, that is, a surface that is digitally patterned at subwavelength dimensions. Enhanced light-matter interactions at the interfaces of the metasurface break the symmetry in the propagation direction, and enables high light-transmission in one direction, while strongly reflecting the light in the opposite direction. We measured a peak extinction ratio of 11.18 dB and peak forward transmission efficiency of 74.3% at the design wavelength of 1.55μm. The operational bandwidth of the device was 201nm. We further designed, fabricated and experimentally characterized a digital metasurface that enables polarization-independent optical-diode behavior, which we believe is the first device of its kind. Our digital metasurfaces enable the optical-diode behavior in a single layer of sub-wavelength thickness for several input modes and therefore, can perform as a passive, albeit imperfect optical isolator.

OCIS codes: (050.1970) Diffractive optics; (350.4238) Nanophotonics and photonic crystals; (350.3950) Micro-optics.

References and links

1. A. S. Schwanecke, V. A. Fedotov, V. V. Khardikov, S. L. Prosvirnin, Y. Chen, and N. I. Zheludev, "Nanostructured metal film with asymmetric optical transmission," Nano Lett. **8**(9), 2940–2943 (2008).
2. E. Plum, V. A. Fedotov, and N. I. Zheludev, "Asymmetric transmission: a generic property of two-dimensional periodic patterns," J. Opt. **13**(2), 024006 (2011).
3. R. A. Shelby, D. R. Smith, and S. Schultz, "Experimental verification of a negative index of refraction," Science **292**(5514), 77–79 (2001).
4. M. Scalora, R. J. Flynn, S. B. Reinhardt, R. L. Fork, M. J. Bloemer, M. D. Tocci, C. M. Bowden, H. S. Ledbetter, J. M. Bendickson, J. P. Dowling, and R. P. Leavitt, "Ultrashort pulse propagation at the photonic band edge: large tunable group delay with minimal distortion and loss," Phys. Rev. E Stat. Phys. Plasmas Fluids Relat. Interdiscip. Topics **54**(2), R1078–R1081 (1996).
5. S. Cakmakyapan, H. Caglayan, A. E. Serebryannikov, and E. Ozbay, "Experimental validation of strong directional selectivity in nonsymmetric metallic gratings with a subwavelength slit," Appl. Phys. Lett. **98**(5), 051103 (2011).
6. S. Cakmakyapan, A. E. Serebryannikov, H. Caglayan, and E. Ozbay, "Spoof-plasmon relevant one-way collimation and multiplexing at beaming from a slit in metallic grating," Opt. Express **20**(24), 26636–26648 (2012).
7. A. Cicek, M. B. Yucel, O. A. Kaya, and B. Ulug, "Refraction-based photonic crystal diode," Opt. Lett. **37**(14), 2937–2939 (2012).
8. L. Wu, Z. Yang, Y. Cheng, M. Zhao, R. Gong, Y. Zheng, J. Duan, and X. Yuan, "Giant asymmetric transmission of circular polarization in layer-by-layer chiral metamaterials," Appl. Phys. Lett. **103**(2), 021903 (2013).
9. C. Menzel, C. Helgert, C. Rockstuhl, E. B. Kley, A. Tünnermann, T. Pertsch, and F. Lederer, "Asymmetric transmission of linearly polarized light at optical metamaterials," Phys. Rev. Lett. **104**(25), 253902 (2010).
10. T. Xu and H. J. Lezec, "Visible-frequency asymmetric transmission devices incorporating a hyperbolic metamaterial," Nat. Commun. **5**, 4141 (2014).
11. M. Kang, J. Chen, H. X. Cui, Y. Li, and H. T. Wang, "Asymmetric transmission for linearly polarized electromagnetic radiation," Opt. Express **19**(9), 8347–8356 (2011).
12. M. Mutlu, A. E. Akosman, A. E. Serebryannikov, and E. Ozbay, "Diodelike asymmetric transmission of linearly polarized waves using magnetoelectric coupling and electromagnetic wave tunneling," Phys. Rev. Lett. **108**(21), 213905 (2012).

#242590 Received 11 Jun 2015; revised 10 Jul 2015; accepted 29 Jul 2015; published 3 Aug 2015

13. A. Mandatori, M. Bertolotti, and C. Sibilia, "Asymmetric transmission of some two-dimensional photonic crystals," J. Opt. Soc. Am. B **24**(3), 685–690 (2007).
14. M. J. Lockyear, A. P. Hibbins, K. R. White, and J. R. Sambles, "One-way diffraction grating," Phys. Rev. E Stat. Nonlin. Soft Matter Phys. **74**(5), 056611 (2006).
15. M. Stolarek, D. Yavorskiy, R. Kotyński, C. J. Zapata Rodríguez, J. Łusakowski, and T. Szoplik, "Asymmetric transmission of terahertz radiation through a double grating," Opt. Lett. **38**(6), 839–841 (2013).
16. V. A. Fedotov, P. L. Mladyonov, S. L. Prosvirnin, A. V. Rogacheva, Y. Chen, and N. I. Zheludev, "Asymmetric propagation of electromagnetic waves through a planar chiral structure," Phys. Rev. Lett. **97**(16), 167401 (2006).
17. A. V. Novitsky, V. M. Galynsky, and S. V. Zhukovsky, "Asymmetric transmission in planar chiral split-ring metamaterials: microscopic Lorentz-theory approach," Phys. Rev. B **86**(7), 075138 (2012).
18. R. Singh, E. Plum, C. Menzel, C. Rockstuhl, A. K. Azad, R. A. Cheville, F. Lederer, W. Zhang, and N. I. Zheludev, "Terahertz metamaterial with asymmetric transmission," Phys. Rev. B **80**(15), 153104 (2009).
19. L. R. Arnaut, "Chirality in multi-dimensional space with application to electromagnetic characterization of multi-dimensional chiral and semi-chiral media," J. Electromagn. Waves Appl. **11**(11), 1459–1482 (1997).
20. S. I. Maslovski, D. K. Morits, and S. A. Tretyakov, "Symmetry and reciprocity constraints on diffraction by gratings of quasi-planar particles," J. Opt. A, Pure Appl. Opt. **11**(7), 074004 (2009).
21. A. Papakostas, A. Potts, D. M. Bagnall, S. L. Prosvirnin, H. J. Coles, and N. I. Zheludev, "Optical manifestations of planar chirality," Phys. Rev. Lett. **90**(10), 107404 (2003).
22. T. Vallius, K. Jefimovs, J. Turunen, P. Vahimaa, and Y. Svirko, "Optical activity in subwavelength-period arrays of chiral metallic particles," Appl. Phys. Lett. **83**(2), 234–236 (2003).
23. A. S. Schwanecke, A. Krasavin, D. M. Bagnall, A. Potts, A. V. Zayats, and N. I. Zheludev, "Broken time reversal of light interaction with planar chiral nanostructures," Phys. Rev. Lett. **91**(24), 247404 (2003).
24. M. Kuwata-Gonokami, N. Saito, Y. Ino, M. Kauranen, K. Jefimovs, T. Vallius, J. Turunen, and Y. Svirko, "Giant optical activity in quasi-two-dimensional planar nanostructures," Phys. Rev. Lett. **95**(22), 227401 (2005).
25. S. Liu, M. B. Sinclair, T. S. Mahony, Y. C. Jun, S. Campione, J. Ginn, D. A. Bender, J. R. Wendt, J. F. Ihlefeld, P. G. Clem, J. B. Wright, and I. Brener, "Optical magnetic mirrors without metals," Optica **1**(4), 250–256 (2014).
26. B. Shen, P. Wang, R. Polson, and R. Menon, "Integrated metamaterials for efficient and compact free-space-to-waveguide coupling," Opt. Express **22**(22), 27175–27182 (2014).
27. B. Shen, P. Wang, R. Polson, and R. Menon, "Ultra-high-efficiency metamaterial polarizer," Optica **1**(5), 356–360 (2014).
28. A. Y. Piggott, J. Lu, T. M. Babinec, K. G. Lagoudakis, J. Petykiewicz, and J. Vučković, "Inverse design and implementation of a wavelength demultiplexing grating coupler," Sci. Rep. **4**, 7210 (2014).
29. G. Kim, J.-A. Dominguez-Caballero, H. Lee, D. J. Friedman, and R. Menon, "Increased photovoltaic power output via diffractive spectrum separation," Phys. Rev. Lett. **110**(12), 123901 (2013).
30. G. Kim and R. Menon, "An ultra-small three dimensional computational microscope," Appl. Phys. Lett. **105**(6), 061114 (2014).
31. B. Shen, P. Wang, R. Polson, and R. Menon, "An integrated-nanophotonics polarization beamsplitter with 2.4 × 2.4 μm2 footprint," Nat. Photonics **9**(6), 378–382 (2015).
32. P. Wang and R. Menon, "Optimization of generalized dielectric nanostructures for enhanced light trapping in thin-film photovoltaics via boosting the local density of optical states," Opt. Express **22**(S1 Suppl 1), A99–A110 (2014).
33. B. Shen, P. Wang, and R. Menon, "Optimization and analysis of 3D nanostructures for power-density enhancement in ultra-thin photovoltaics under oblique illumination," Opt. Express **22**(102), A311–A319 (2014).
34. A. F. Oskooi, D. Roundy, M. Ibanescu, P. Bermel, J. D. Joannopoulos, and S. G. Johnson, "MEEP: A flexible free-software package for electromagnetic simulations by the FDTD method," Comput. Phys. Commun. **181**(3), 687–702 (2010).
35. D. Jalas, A. Petrov, M. Eich, W. Freude, S. Fan, Z. Yu, R. Baets, M. Popović, A. Melloni, J. D. Joannopoulos, M. Vanwolleghem, C. R. Doerr, and H. Renner, "What is and what is not an optical isolator," Nat. Photonics **7**(8), 579–582 (2013).
36. M. Stolarek, D. Yavorskiy, R. Kotyński, C. J. Zapata Rodríguez, J. Łusakowski, and T. Szoplik, "Asymmetric transmission of terahertz radiation through a double grating," Opt. Lett. **38**(6), 839–841 (2013).
37. R. Singh, E. Plum, C. Menzel, C. Rockstuhl, A. K. Azad, R. A. Cheville, F. Lederer, W. Zhang, and N. I. Zheludev, "Terahertz metamaterial with asymmetric transmission," Phys. Rev. B **80**(15), 153104 (2009).

1. Introduction

Metamaterials are artificially structured materials that are engineered to exhibit extraordinary electromagnetic responses, e.g. asymmetric transmission [1,2], negative index [3] and ultra-slow speed of light [4], that are not found in natural materials. Asymmetric transmission or optical-diode behavior is one such property that has recently been studied due to its potential applications in directionally-sensitive beam splitting [5], multiplexing [6], and optical interconnection [7]. The asymmetric transmission of both circular and linearly polarized light in three-dimensional (3D) volumetric metamaterials have been widely reported [8–12]. Bi-

#242590 Received 11 Jun 2015; revised 10 Jul 2015; accepted 29 Jul 2015; published 3 Aug 2015

layered chiral metamaterials consisting of periodic split-rings were used to demonstrate asymmetric transmission of circular polarized light [8]. 3D chiral metamaterials consisting of a layer of L-shaped metallic particles and another layer of straight nanowires were used to demonstrate asymmetric transmission of linearly polarized light [9]. A hyperbolic metamaterial that behaves as an optical diode for linear polarized light at visible frequencies was recently reported [10]. Besides volumetric metamaterials, bulky gratings were also employed to achieve asymmetric transmission [13–15]. The combination of a one-dimensional (1D) photonic bandgap structure and a two-dimensional (2D) periodic multilayer grating was employed to achieve unidirectional transmission [13]. In addition, employing four cascaded air-filled metal slits, Lockyear et. al. showed asymmetric transmission [14]. However, fabrication and alignment associated with all these 3D devices are challenging. Besides, the parasitic absorption of metal significantly reduces their transmission efficiency. For the device proposed by Lockyear et. al., the insertion loss is around −4dB [14]. Another recent demonstration of optical-diode behavior utilized a planar chiral metamaterial (a chiral metasurface), which considerably simplified the fabrication and alignment challenges associated with the 3D metamaterials [16]. Other examples of 2D optical diodes for circular polarized light have also been reported [1,17,18]. These devices operate under the principle of symmetry breaking for circular polarized light in the transverse direction [1,2,18]. However, such symmetry breaking is more difficult for linearly polarized light, although it does not violate Lorentz's reciprocity theorem. Chiral metasurfaces preserves symmetry in the propagation direction and they are only chiral in the transverse plane [19]. Therefore, they do not exhibit asymmetric transmission for linear polarized light. However, it has been reported that the supporting substrate can break the mirror symmetry for any planar structure perpendicular to the propagation direction [20]. Furthermore, by introducing giant optical activity in metasurfaces, it is possible to have them behave as effective 3D metamaterials [21–24]. The enhanced light-matter interaction results in significant nonlocal optical effects seeded by the small, but finite asymmetry at the air-metasurface and the metasurface-substrate interfaces. Using these ideas, polarization rotation of linearly polarized light using chiral metasurfaces have been demonstrated [21]. Broken time reversal of light propagation at chiral metasurfaces has also been demonstrated previously [23]. These demonstrations utilized metals or other lossy materials. However, the principle of symmetry breaking is valid for lossless systems as well [9], as long as giant optical activity is introduced. Recently, it was proposed that enhanced light-matter interactions are feasible at low-loss all-dielectric metasurfaces [25].

Here, we realize asymmetric transmission of linearly polarized light using a dielectric (lossless) metasurface employing the concept of digital metamaterials [26–28]. In fact, our device is not only lossless, but CMOS compatible as well. The insertion loss of previous such devices that incorporate metals is in the order of −10dB [10]. While the insertion loss for our dielectric metasurface is estimated to be −1.3dB. Furthermore, our device considerably simplifies the fabrication process, since only a single etch step is required, and metal deposition or precise alignment steps can be avoided. Asymmetric transmission in the THz or microwave regions have been widely reported, but not in the infra-red (IR). Our device operates at the very useful IR wavelength of ~1550nm. Here, we note that our device is a passive device and hence, does not break Lorentz symmetry. As a result, it works only for a limited incidence angle range (~15°, as discussed later). A perfect optical isolator, which exhibits asymmetric transmission for all incidence angles, requires nonlinearities. However, the divergence angle of Gaussian beams in many practical applications is typically less than 15° and our device could be quite useful in these cases. The basic premise of digital metamaterials is that via nanofabrication, one can control the local refractive index. By spatial engineering of the refractive index at subwavelength dimensions, it is possible to design structures, whose dispersion properties can be engineered efficiently, for instance to enable high-efficiency polarizers [27], ultra-compact devices [26], or strong light-material

#242590 Received 11 Jun 2015; revised 10 Jul 2015; accepted 29 Jul 2015; published 3 Aug 2015

interactions. Furthermore, these devices rely on the coupling between multiple resonant modes, which promotes robustness to fabrication errors, as discussed later. Here, we extend the idea of digital metamaterials to patterned 2D surfaces or digital metasurfaces. Specifically, we designed a digital metasurface that allows linearly polarized light to propagate in one direction but not in the opposite direction. Our device is made of etched silicon and is comprised of a unit cell that is tiled across the 2D plane. The designed structure of one unit cell is illustrated in Fig. 1(a). For computational simplicity, we chose our unit cell to be 4μm × 4μm comprising of 20 × 20 pixels, each pixel of size 200nm × 200nm. The designed etch depth is 330nm, which is considerably smaller than the design free-space wavelength, 1550nm. The simulated steady-state intensity distributions at 1550nm for the forward and the backward directions are shown in Figs. 1(b) and 1(c), respectively. We calculated the extinction ratio, defined as the ratio of transmission efficiency in the forward direction to that in the backward direction, of 14.8dB. This is at least comparable to, if not better than, those previously reported for linear polarization [1,9–11].

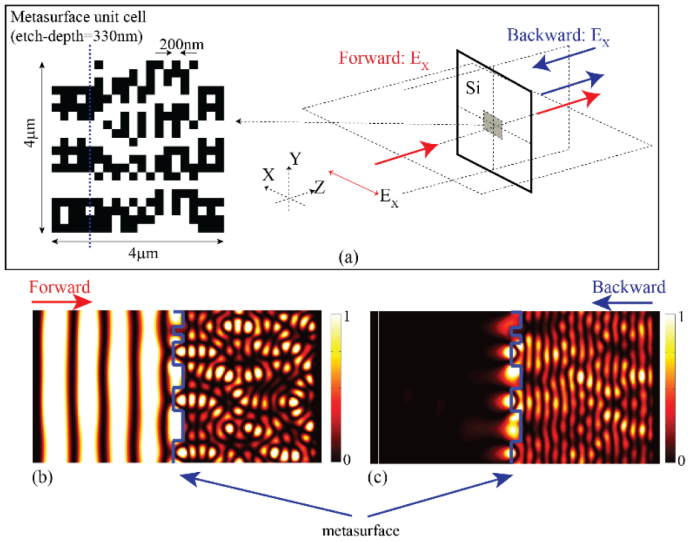

Fig. 1. (a) Metasurface design for asymmetric transmission of linearly polarized light. The design (left) is composed of etched square pixels in silicon. Simulated steady-state intensity distributions in the YZ plane for (b) forward and (c) backward propagation directions (see Visualization 1). Blue dashed line in (a) indicates the location of the YZ cut plane. The blue solid lines in (b) and (c) indicate the location of the metasurface.

2. Design

We applied a modified version of the direct-binary-search (DBS) algorithm to design the metasurface. We have previously used DBS to design non-imaging optics [29,30], free space polarizers [27], integrated devices [26,31] and nanophotonic light-trapping structures [32,33]. The optimization variables are the state of each of the 400 pixels (air or silicon) and the etch depth of all the pixels (note that they are uniformly etched for ease of fabrication). We further constrained the largest aspect ratio of our device (ratio of etch depth to pixel size) to 2 to further simplify the fabrication. Higher aspect ratios can enable better results, however, they increase fabrication complexity. The optimization figure-of-merit (FOM) was the extinction ratio. DBS operates in an iterative fashion. All the parameters including 400 pixels and etch depth are traversed in a random order during one iteration. Proper termination conditions such as minimum FOM improvement is imposed on the optimization to ensure convergence. The basic version of our algorithm is detailed in [26] and the flow chart is shown in Fig. 2. Because of its potential for premature convergence to local maxima, we repeat the search

#242590 Received 11 Jun 2015; revised 10 Jul 2015; accepted 29 Jul 2015; published 3 Aug 2015

algorithm with different starting points. The result with largest FOM is presented here for discussion. Note that fabrication constraints are naturally incorporated into the design due to the discrete nature of the pixels. The choice of pixel size is driven by the capability of the fabrication tool. We take advantage of Amazon's EC2 cloud computing service to expedite the optimization process. The search algorithm was parallelized in a microcluster consisting of three virtual machines. Each machine has 32 virtual CPUs. One optimization typically takes ~480 hours, which can be reduced by employing a larger cluster. An open-source finite-difference time-domain (FDTD) solver (MEEP) was used to simulate the full 3D geometry of our designs [34]. Periodic boundary conditions were applied at the boundaries of the unit cell.

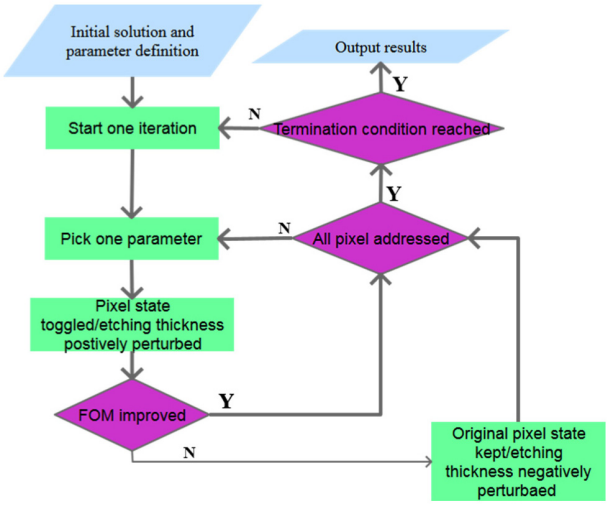

Fig. 2. Flow chart of DBS algorithm.

3. Experiments

In order to characterize the digital metasurface, we illuminated it with collimated linearly polarized light from a NIR laser centered at 1550nm. Opaque gold masks surrounded the metasurface, which blocked the incident light outside the device. The gold windows were slightly larger than the device for ease of alignment. The transmitted power was collected using an imaging lens and a standard photodiode germanium power sensor. A conventional polarizer was placed between the lens and the detector to select the polarization state of the signal. A half-wave plate and a polarizer were used at the input to first align the direction of polarization to the X-axis of the digital metasurface. The measurement setup is illustrated in Fig. 3.

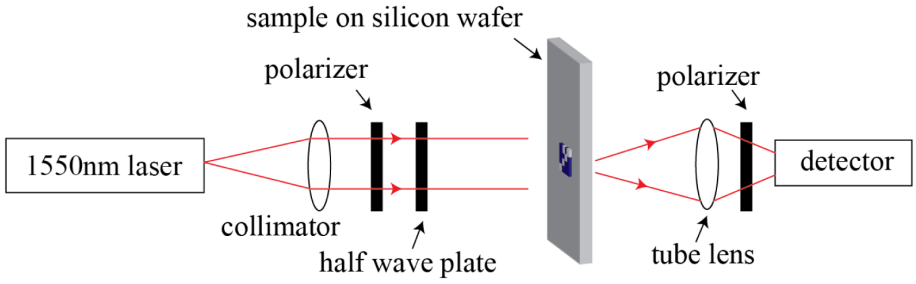

Fig. 3. Schematic of the experimental setup for the asymmetric transmission meta-surface measurements in transmission.

#242590 Received 11 Jun 2015; revised 10 Jul 2015; accepted 29 Jul 2015; published 3 Aug 2015

The digital metasurface was fabricated by etching into silicon using focused-ion-beam lithography. We used an ion beam energy of 30kV and current of 7.7pA to etch the structures with a target depth of 330nm. Details of the fabrication process were previously reported in [26]. Figure 4(a) shows the scanning-electron micrograph of a fabricated device composed of 4 × 4 unit cells, where each unit cell is 4μm × 4μm (denoted by dashed red lines). A magnified view of one unit cell is shown in Fig. 4(b).

Our metasurface is patterned on one side of a double-side polished Si substrate. We used an unpatterned double-side polished Si substrate as the reference. The measured and the simulated forward and backward transmission efficiencies, normalized to the transmitted intensities of the reference (we refer to this as the transmission enhancement), are shown in Fig. 4(c). The experiments cover the tunable bandwidth of our laser source, while the simulations cover a much larger bandwidth. Although there are small discrepancies between the measured and the simulated values, they agree well overall. The discrepancies are likely due to the small polarization state misalignment and sub-optimal light coupling between the metasurface and the detector. We measured an extinction ratio of 11.18dB at 1550nm. The transmission enhancement at the design wavelength (1.55μm) is measured to be 1.07, which corresponds to an absolute transmission efficiency of 74.3% and an insertion loss of −1.3dB. Note that the measured transmission enhancement is larger than 1 at some wavelengths. This means that light transmission is enhanced at the meta-surface when compared to the unpatterned Si wafer.

From the simulated transmission enhancement plot shown in Fig. 4(c), the 3dB bandwidth (where the extinction ratio is higher than half of the peak value) of the metasurface is estimated to be 201nm (1420nm to 1621nm). Compare this to a previously reported device, whose bandwidth is only tens of nanometers [10]. Our device exhibits larger bandwidth due to the fact that coherent interactions between multiple coupled guided modes is responsible for the asymmetric transmission. The multiple resonances enable the device to be less sensitive to wavelength shifts.

We also numerically investigated the device's sensitivity to fabrication errors. Specifically, we varied the etch depth of the metasurface and calculated the forward and backward transmission enhancement spectra as shown in Fig. 4(d). If we can tolerate a 3dB drop of extinction ratio from the peak value, we can allow the etch depth of the metasurface to vary by as much as 95nm (−15nm to 80nm). Therefore, our digital metasurface is highly tolerant to fabrication errors as well.

Although our device was designed for normal incidence, we simulated the impact of oblique incidence (or higher order modes) on the performance of the device. Since the metasurface is anisotropic in transverse plane, we investigate its performance under oblique incidence with projection both on X axis and Y axis as illustrated in Fig. 5. Figure 5(a) shows the extinction ratio as a function of incident angle for k vector projection both on X and Y axis. The two types of oblique incident angle are illustrated in Fig. 5(b). For k_x, an angle variation of 15° about the normal would bring a 3dB drop of the extinction ratio. While for k_y, the corresponding angle variation is 10°.

#242590 Received 11 Jun 2015; revised 10 Jul 2015; accepted 29 Jul 2015; published 3 Aug 2015

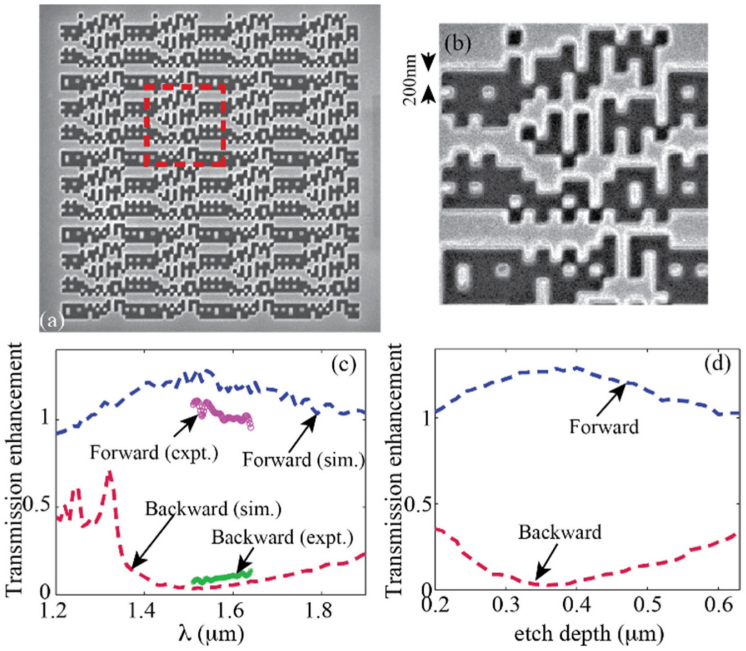

Fig. 4. (a) Scanning-electron micrograph of the fabricated metasurface. One unit cell is 4μm × 4μm as shown by the red dashed lines, and the device consists of 4 × 4 unit cells. (b) Scanning-electron micrograph of one unit cell. (c) Measured and simulated transmission enhancement with respect to an unpatterned Si substrate as a function of wavelength. (d) Simulated transmission enhancement with respect to an unpatterned Si substrate as a function of the etch depth.

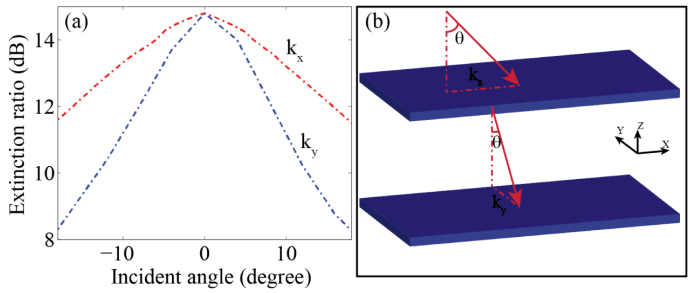

Fig. 5. Performance analysis under oblique illumination for metasurface for linearly polarized light. (a) Extinction ratio as a function of incident angles for k_x and k_y. (b) Illustration of two types oblique illumination: k_x and k_y.

4. Explanation

We also simulated the time evolution of the electric field within the metasurface for linearly polarized light in order to visualize its performance. The resulting animation is included as supplementary information. Due to the subwavelength structures within the device, guided resonance modes are excited within the metasurface. For forward direction, propagating modes are excited at the metasurface-silicon interface and propagate readily into silicon (see Visualization 1). For the backward direction, primarily evanescent modes are excited at the metasurface-air interface, and therefore, penetrate only a small distance into the air (see Visualization 1). This asymmetry gives rise to the drastic difference in transmission efficiencies in the two directions.

#242590 Received 11 Jun 2015; revised 10 Jul 2015; accepted 29 Jul 2015; published 3 Aug 2015

The specific arrangement of pixels in our digital metasurface interact with incident light such that the excited guided-mode resonances result in light propagation in only one direction. This can be contrasted against a completely random digital metasurface, where no such asymmetric-light transmission is observed, which is shown in Fig. 6. Furthermore, the guided-mode resonances in the designed digital metasurface leads to giant light-matter interactions at the two interfaces, (see Figs. 6(c)-6(d)) which results in strong nonlocal effects seeded by the small but finite asymmetry at the interfaces. Governed by the phase-matching condition at the air-metasurface interface, guided-mode resonances excite evanescent modes that penetrate a small distance into the air (as shown in Fig. 6(b)). On the other hand, at the metasurface-Si interface, the guided-mode resonances excite propagating modes into Si as shown in Fig. 6(a). Note that the device has no absorption losses.

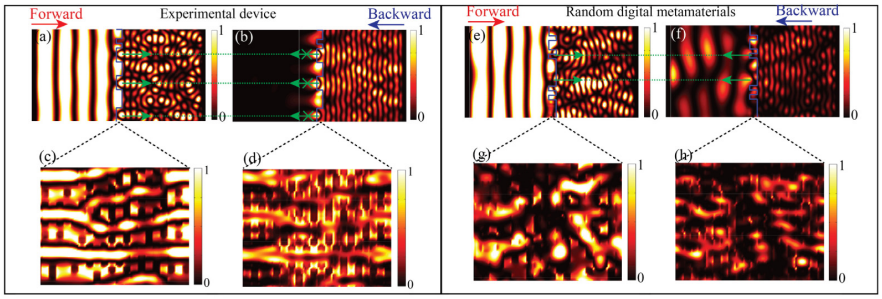

Fig. 6. Simulated steady-state electric intensity pattern for experimental device (for linearly polarized light) and random digital metamaterials. Field pattern in YZ plane for (a) forward and (b) backward direction of experimental device. Field pattern at (c) air-metamaterial and (d) metamaterial-silicon interface (XY plane) for experimental device. Field pattern in YZ plane for (e) forward and (f) backward direction of random digital metamaterials. Field pattern in (g) air-metamaterial and (h) metamaterial-silicon interface (XY plane) for random digital metamaterials. In all the plot, Z is the light propagation direction. Green arrows indicate light propagation direction and cross at arrows means that light decays fast after the meta-surface. Blue solid line indicate the epsilon distribution of the meta-surface.

5. Polarization independent optical diode

We also designed and experimentally characterized a polarization independent optical diode using the concept of digital metasurfaces. Asymmetric transmission of light with either of the two linear orthogonal polarization states is achieved at the digital metasurface. Figure 7(a) shows the scanning-electron micrograph of the fabricated metasurface composed of 4 × 4 unit cells, each of size 4μm × 4μm. The measured as well as simulated transmission enhancement with respect to unpatterned Si as a function of wavelength for both polarizations are shown in Fig. 7(b). The inset in Fig. 7(b) shows the device design (one unit cell). The simulated steady-state intensity distributions at both polarizations for the forward and the backward propagation directions at the design wavelength (1.55μm) are shown in Figs. 7(c)-7(f). The measurements confirm extinction ratios of 10.8dB and 9.1dB at $\lambda = 1.55\mu m$ for E_x and E_y, respectively. In comparison, the simulated extinction ratios are 13.3dB and 12.3dB for E_x and E_y, respectively. The discrepancies between simulations and measurements are likely due to a combination of the misalignment of the polarization state and sub-optimal light coupling from metasurface to the receiver. As far as we are aware, this is the first report of a device that enables polarization-independent asymmetric transmission. The time evolution of the electric fields within this device is included as supplementary video (Visualization 2).

#242590 Received 11 Jun 2015; revised 10 Jul 2015; accepted 29 Jul 2015; published 3 Aug 2015

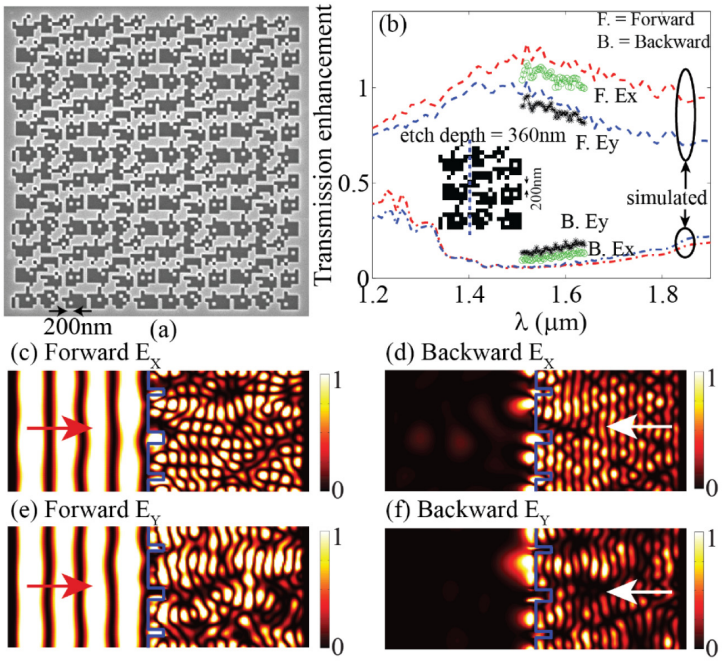

Fig. 7. Polarization independent asymmetric transmission. (a) Scanning-electron micrograph of the fabricated digital metasurface. The fabricated device consists of 4 by 4 unit cells, each of size, 4μm × 4μm. (b) Measured and simulated transmission enhancement with respect to unpatterned Si as a function of wavelength. Lines with markers represent measurement data, while lines without markers represent simulation data. Red and blue lines represent the calculated transmission-enhancement spectra for E_x and E_y, respectively. Inset shows the design of the digital metasurface. (c)-(f) Simulated steady-state intensity distributions in the YZ plane of E_x and E_y polarized light in the forward and backward directions (see Visualization 2). The blue dashed line in (b) indicates the YZ cut-plane used for the simulations in (c)-(f). The blue solid lines in (c)-(f) indicate the location of the digital metasurface.

6. Conclusion

In conclusion, we introduce the concept of digital metasurfaces, 2D devices comprised of etched discrete pixels, whose photonic functionality can be tailored via fabrication-constrained numerical optimization. Specifically, we designed, fabricated and characterized digital metasurfaces to exhibit optical-diode behavior or asymmetric transmission of linearly polarized light. The digital metasurfaces have no absorption losses, are relatively easy to fabricate (CMOS compatible and require only a single lithography step), are robust to fabrication errors, and exhibit excellent transmission efficiencies, extinction ratios and operational bandwidths. Polarization-independent asymmetric transmission is also demonstrated. Enhanced light-matter interactions are achieved via a directed design of the subwavelength structures, which when combined with the interfacial asymmetries result in the optical-diode behavior. It is important to point out that our devices are completely reciprocal in the Lorentz sense [35] and therefore, cannot be used a perfect optical isolator. Nevertheless, simulations indicate that the digital metasurface has an acceptance angle as large as 15°, and therefore, could be used for optical isolation as long as the incident modes are restricted. Furthermore, such optically asymmetric devices could have important applications in filters, direction sensitive beam splitters, circulators and sensor components [36,37].

#242590 Received 11 Jun 2015; revised 10 Jul 2015; accepted 29 Jul 2015; published 3 Aug 2015

Acknowledgments

We wish to thank Jose Dominguez-Caballero for assistance with the direct binary-search algorithm, Brian Baker for assistance with sample preparation, and Ganghun Kim for assistance with the measurement setup. We thank Peng Wang for useful discussions about FDTD simulation and Steve Blair for use of the tunable fiber laser. This work made use of University of Utah shared facilities of the Micron Technology Foundation Inc. Microscopy Suite sponsored by the College of Engineering, Health Sciences Center, Office of the Vice President for Research, and the Utah Science Technology and Research (USTAR) initiative of the State of Utah. This work made use of University of Utah USTAR shared facilities supported, in part, by the MRSEC Program of the NSF under Award No. DMR-1121252. Authors thank funding support from National Aeronautics and Space Administration (NASA) (NNX14AB13G), U.S. Department of Energy (DOE) (EE0005959), and University of Utah.

#242590 Received 11 Jun 2015; revised 10 Jul 2015; accepted 29 Jul 2015; published 3 Aug 2015